RC76 Phelan, M., and LoVetri, J. (2004) *Polarimetric Bistatic GPR Imaging and Detection of Landmines in the Near Field with the "Vampire Effect"*, Proceedings of ANTEM'2004/URSI, pp. 77-81, Ottawa, Canada, July 20 - 23.

POLARIMETRIC BISTATIC GPR IMAGING AND DETECTION OF LANDMINES IN THE NEAR FIELD WITH THE "VAMPIRE EFFECT"

Michael Phelan*, Joe LoVetri**
University of Manitoba, Winnipeg, Canada
*mphelan@ee.umanitoba.ca **lovetri@ee.umanitoba.ca

Abstract — GPR images invariably suffer from a bandwidth restriction due to the low pass characteristics of the air-ground interface and are usually not clear enough to differentiate between what is a landmine and what is harmless clutter. The presence of clutter in the subsurface therefore contributes to high false alarm rates when landmine detection schemes are attempted. A landmine detection algorithm based on the vampire signature has been proposed and has been tested to verify its validity. The method involves the construction of a spatial filter from polarimetric data in order to enhance objects that exhibit the vampire effect while suppressing objects that do not. So far, the method has several significant limitations, most notably that the position and orientation of the symmetric scatters is strictly confined to be directly below the SAR path and that the target symmetry planes must include both antennas as well as the scan path. In this paper, the effects of off-centered measurements whereby the antennas are not necessarily contained in the target symmetry plane are discussed.

INTRODUCTION

Previous experiments [1] have shown that the vampire effect can be exploited in bistatic near field measurements to create a spatial filter that enhances the response from symmetrical targets when the target response is measured by a bistatic pair confined to the target symmetry plane. The concept is an extension of the so called vampire signature effect introduced by Baum [2][3] whereby the monostatic backscattered fields measured from a point on the target symmetry plane exhibit no cross-polarized response in the far field. The principle is applied to GPR in a series of polarimetric SAR measurements to differentiate between buried landmines, which are generally geometrically symmetric, and random clutter, which is generally asymmetric. The vampire signature can then be considered as a feature to discriminate between landmines from subsurface clutter. The constraint that the bistatic antenna pair always reside in a target symmetry plane in order to generate nulls in the cross polarization response is restrictive in the sense that the location of a target symmetry plane must be known a priori on order to take advantage of the vampire signature for SAR measurements. For practical landmine detection purposes, it can not be assumed that the location and orientation of the target symmetry planes are known in advance, therefore the effects of bistatic measurements taken when the antenna pair are not located on the target symmetry plane requires investigation. Preliminary experiments suggest that the vampire signature can be an effective feature in landmine detection under ideal conditions (i.e. that the locations and orientations of the target symmetry planes are known a priori), here the effects of GPR measurements taken along SAR paths that are not contained in the target symmetry plane are discussed.

FORMULATION

In order to study the concept of symmetry, it is advantageous to use mathematical group theory in the formulations since it is a tool that is particularly useful for describing and exploiting symmetry.

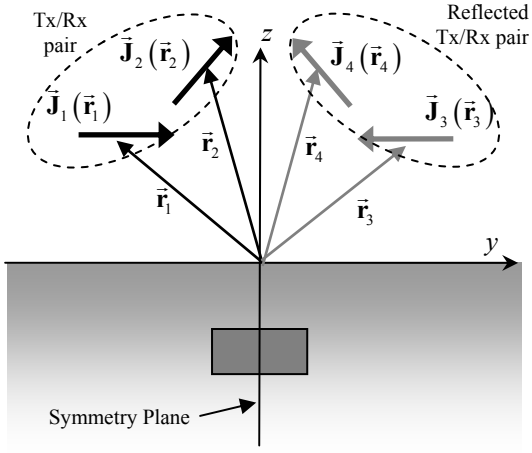

Figure 1: A target with a symmetry plane appears identical to measurements taken at positions reflected through the plane.

Consider a target with a symmetry plane such that the object is invariant to reflection operation through the *x-z* plane as shown in Figure 1, meaning that the object appears exactly the same through a reflection of the observation point if a "mirror" were to be placed in the *x-z* plane. The symmetry of this object is said to have a matrix representation $\vec{\mathbf{R}}$ with respect to the symmetry plane such that in the $\langle \hat{\mathbf{e}}_x, \hat{\mathbf{e}}_y, \hat{\mathbf{e}}_z \rangle$ Cartesian basis, $\vec{\mathbf{R}}$ can be written as

$$\vec{\mathbf{R}} = \begin{bmatrix} 1 & 0 & 0 \\ 0 & -1 & 0 \\ 0 & 0 & 1 \end{bmatrix} \qquad (1)$$

This matrix representation transforms the coordinates of the position vectors as

$$\vec{\mathbf{r}}_3 = \overleftrightarrow{\mathbf{R}} \bullet \vec{\mathbf{r}}_1 \quad \longrightarrow \quad \vec{\mathbf{r}}_1 = \overleftrightarrow{\mathbf{R}}^{-1} \bullet \vec{\mathbf{r}}_3$$
$$\vec{\mathbf{r}}_4 = \overleftrightarrow{\mathbf{R}} \bullet \vec{\mathbf{r}}_2 \quad \longrightarrow \quad \vec{\mathbf{r}}_2 = \overleftrightarrow{\mathbf{R}}^{-1} \bullet \vec{\mathbf{r}}_4 \tag{2}$$

In conventional *h*, *v* radar coordinates, a basis vector forms a right handed system with $\langle \hat{\mathbf{e}}_h, \hat{\mathbf{e}}_v, -\hat{\mathbf{e}}_i \rangle$ where $\hat{\mathbf{e}}_i$ is the direction of incidence in the far field as shown in Figure 2.

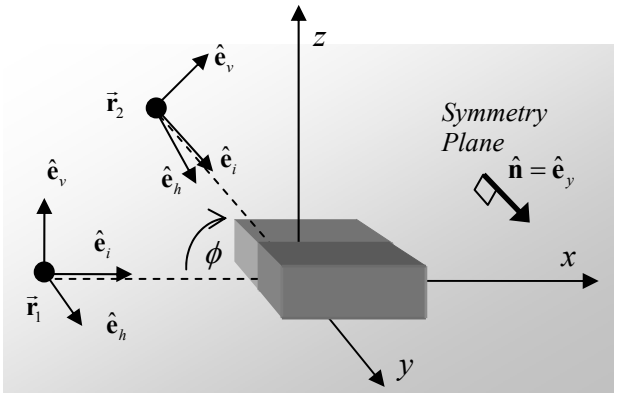

Figure 2: Target with a symmetry plane undergoing a bistatic measurement in the symmetry plane.

The dyadic Green's function in this coordinate system is given as

$$\overline{\overline{\mathbf{G}}}(\vec{\mathbf{r}}_1, \vec{\mathbf{r}}_2) = \begin{bmatrix} g_{hh}(\vec{\mathbf{r}}_1, \vec{\mathbf{r}}_2) & g_{hv}(\vec{\mathbf{r}}_1, \vec{\mathbf{r}}_2) & g_{hi}(\vec{\mathbf{r}}_1, \vec{\mathbf{r}}_2) \\ g_{vh}(\vec{\mathbf{r}}_1, \vec{\mathbf{r}}_2) & g_{vv}(\vec{\mathbf{r}}_1, \vec{\mathbf{r}}_2) & g_{vi}(\vec{\mathbf{r}}_1, \vec{\mathbf{r}}_2) \\ g_{ih}(\vec{\mathbf{r}}_1, \vec{\mathbf{r}}_2) & g_{iv}(\vec{\mathbf{r}}_1, \vec{\mathbf{r}}_2) & g_{ii}(\vec{\mathbf{r}}_1, \vec{\mathbf{r}}_2) \end{bmatrix} \tag{3}$$

where $\overline{\overline{\mathbf{G}}}(\vec{\mathbf{r}}_1, \vec{\mathbf{r}}_2)$, and a similar equation for $\overline{\overline{\mathbf{G}}}(\vec{\mathbf{r}}_3, \vec{\mathbf{r}}_4)$, satisfies the solution of the vector wave equation for a bistatic measurement such that the scattered fields at $\vec{\mathbf{r}}_2$ and $\vec{\mathbf{r}}_4$ due to sources present at $\vec{\mathbf{r}}_1$ and $\vec{\mathbf{r}}_3$, denoted as $\vec{\mathbf{E}}^{(s)}$ can be written as

$$\vec{\mathbf{E}}_2^{(s)}(\vec{\mathbf{r}}_2) = -j\omega\mu \iiint_{V_1} \overline{\overline{\mathbf{G}}}(\vec{\mathbf{r}}_1, \vec{\mathbf{r}}_2) \bullet \vec{\mathbf{J}}_1(\vec{\mathbf{r}}_1)\, d\vec{\mathbf{r}}_1 \tag{4}$$

$$\vec{\mathbf{E}}_4^{(s)}(\vec{\mathbf{r}}_4) = -j\omega\mu \iiint_{V_3} \overline{\overline{\mathbf{G}}}(\vec{\mathbf{r}}_3, \vec{\mathbf{r}}_4) \bullet \vec{\mathbf{J}}_3(\vec{\mathbf{r}}_3)\, d\vec{\mathbf{r}}_3 \tag{5}$$

Due to symmetry we have

$$\vec{\mathbf{E}}_4^{(s)}(\vec{\mathbf{r}}_4) = \overleftrightarrow{\mathbf{R}} \bullet \vec{\mathbf{E}}_2^{(s)}(\vec{\mathbf{r}}_2) \tag{6}$$

If the position vectors are eigenvectors of the matrix representation that correspond to unit valued eigenvalues, the vectors are said to be degenerate and will be invariant with respect to operations of $\overleftrightarrow{\mathbf{R}}$, meaning that the degenerate vectors are not changed by the symmetry operation [4]. This implies that if $\vec{\mathbf{r}}_1$ and $\vec{\mathbf{r}}_2$ are degenerate,

$$\vec{\mathbf{r}}_1 = \overleftrightarrow{\mathbf{R}} \bullet \vec{\mathbf{r}}_1, \quad \vec{\mathbf{r}}_2 = \overleftrightarrow{\mathbf{R}} \bullet \vec{\mathbf{r}}_2 \tag{7}$$

Therefore we can write

$$\begin{aligned} &\overleftrightarrow{\mathbf{R}} \bullet \vec{\mathbf{E}}_2^{(s)}(\vec{\mathbf{r}}_2) \\ &= -j\omega\mu \iiint_{V_1} \overleftrightarrow{\mathbf{R}} \bullet \overline{\overline{\mathbf{G}}}(\vec{\mathbf{r}}_1, \vec{\mathbf{r}}_2) \bullet \vec{\mathbf{J}}_1(\vec{\mathbf{r}}_1)\, d\vec{\mathbf{r}}_1 \\ &= -j\omega\mu \iiint_{V_1} \overleftrightarrow{\mathbf{R}} \bullet \overline{\overline{\mathbf{G}}}(\vec{\mathbf{r}}_1, \vec{\mathbf{r}}_2) \bullet \overleftrightarrow{\mathbf{R}}^{-1} \bullet \overleftrightarrow{\mathbf{R}} \bullet \vec{\mathbf{J}}_1(\vec{\mathbf{r}}_1)\, d\vec{\mathbf{r}}_1 \\ &= -j\omega\mu \iiint_{V_3} \left(\overleftrightarrow{\mathbf{R}} \bullet \overline{\overline{\mathbf{G}}}\left(\overleftrightarrow{\mathbf{R}}^{-1} \bullet \vec{\mathbf{r}}_3, \overleftrightarrow{\mathbf{R}}^{-1} \bullet \vec{\mathbf{r}}_4 \right) \bullet \overleftrightarrow{\mathbf{R}}^{-1} \right) \bullet \vec{\mathbf{J}}_3(\vec{\mathbf{r}}_3)\, d\vec{\mathbf{r}}_3 \\ &= \vec{\mathbf{E}}_4^{(s)}(\vec{\mathbf{r}}_4) \end{aligned} \tag{8}$$

This leads to the following statement which can be considered a generalized form of electromagnetic reciprocity for symmetric scatterers [5]

$$\overline{\overline{\mathbf{G}}}(\vec{\mathbf{r}}_a, \vec{\mathbf{r}}_b) = \overleftrightarrow{\mathbf{R}} \bullet \overline{\overline{\mathbf{G}}}\left(\overleftrightarrow{\mathbf{R}}^{-1} \bullet \vec{\mathbf{r}}_a, \overleftrightarrow{\mathbf{R}}^{-1} \bullet \vec{\mathbf{r}}_b \right) \bullet \overleftrightarrow{\mathbf{R}}^{-1} \tag{9}$$

If the position vectors are degenerate with respect to the matrix representation as in (7), then the following simplification can be made

$$\begin{aligned} \overline{\overline{\mathbf{G}}}(\vec{\mathbf{r}}_1, \vec{\mathbf{r}}_2) &= \overleftrightarrow{\mathbf{R}} \bullet \overline{\overline{\mathbf{G}}}(\vec{\mathbf{r}}_1, \vec{\mathbf{r}}_2) \bullet \overleftrightarrow{\mathbf{R}}^{-1} \\ &= \begin{bmatrix} g_{hh}(\vec{\mathbf{r}}_1, \vec{\mathbf{r}}_2) & -g_{hv}(\vec{\mathbf{r}}_1, \vec{\mathbf{r}}_2) & g_{hi}(\vec{\mathbf{r}}_1, \vec{\mathbf{r}}_2) \\ -g_{vh}(\vec{\mathbf{r}}_1, \vec{\mathbf{r}}_2) & g_{vv}(\vec{\mathbf{r}}_1, \vec{\mathbf{r}}_2) & -g_{vi}(\vec{\mathbf{r}}_1, \vec{\mathbf{r}}_2) \\ g_{ih}(\vec{\mathbf{r}}_1, \vec{\mathbf{r}}_2) & -g_{iv}(\vec{\mathbf{r}}_1, \vec{\mathbf{r}}_2) & g_{ii}(\vec{\mathbf{r}}_1, \vec{\mathbf{r}}_2) \end{bmatrix} \end{aligned} \tag{10}$$

Equating (10) and (3), it is apparent that for the case when both antennas are on the target's symmetry plane the dyadic Green's function can be rewritten as

$$\overline{\overline{\mathbf{G}}}(\vec{\mathbf{r}}_1, \vec{\mathbf{r}}_2) = \begin{bmatrix} g_{hh}(\vec{\mathbf{r}}_1, \vec{\mathbf{r}}_2) & 0 & g_{hi}(\vec{\mathbf{r}}_1, \vec{\mathbf{r}}_2) \\ 0 & g_{vv}(\vec{\mathbf{r}}_1, \vec{\mathbf{r}}_2) & 0 \\ g_{ih}(\vec{\mathbf{r}}_1, \vec{\mathbf{r}}_2) & 0 & g_{ii}(\vec{\mathbf{r}}_1, \vec{\mathbf{r}}_2) \end{bmatrix} \tag{11}$$

If the incident wave is polarized in the *h* direction, there will be no cross polarization in the *v* direction and conversely, if the incident wave is polarized in the *v* direction, there will be no cross polarization in the *h* direction. This principle can be applied to collected GPR data to verify if the target possesses a dyadic Green's function of the form of (11). If it does, the target can be assumed to be an object with a symmetry plane measured from antennas positioned on this plane.

PROPOSED ALGORITHM

To take advantage of the vampire effect for targets that are measured by antennas on the target symmetry plane, a simple spatial filtering algorithm has been developed. Target information is gathered by means of a stepped

frequency GPR system along a linear synthetic aperture for all three polarizations *hh*, *vv* and *hv*. The resulting data is processed using the frequency-wavenumber (FK) migration algorithm in conjunction with a Hanning window in the frequency domain [6] in order to render the data into images of the subsurface in the range and cross-range directions. The complex valued images, I_{hh}, I_{vv} and I_{hv} correspond to polarimetric representations of the subsurface. Because of conventional reciprocity, i.e. $g_{hv} = g_{vh}$, only the one cross-polarization term, I_{hv} is required. Since, for images, only relative intensities are of concern, the absolute values of the images, normalized to unity with respect to their respective maximum values, $\left|\tilde{I}_{hh}\right|$, $\left|\tilde{I}_{vv}\right|$ and $\left|\tilde{I}_{hv}\right|$ are computed where the ~ overbar denotes normalization to unity. All three images are then restricted to values between zero and unity.

Lack of a cross-polarization in the target according to (11) is taken to be a sign of symmetry for the target (if the bistatic pair is located on the target's symmetry plane). A spatial filter, *F*, can then be constructed from the normalized cross-polarization information as

$$\tilde{F} = 1 - \left|\tilde{I}_{hv}\right| \tag{12}$$

Since $0 \geq \left|\tilde{I}_{hv}\right| \geq 1$, *F* will also be relegated to values between zero and unity but will posses minimums at regions of high cross-polarization (lack of symmetry) and maximums at regions of low cross-polarization (symmetric regions).

The spatial polarization filter *F* is then blurred slightly by means of a normalized 2D convolution filter where the convolution kernel is a disk, k_d, with a pre-selected radius:

$$\tilde{F}' = \frac{\tilde{F} * k_d}{\max\left\{\tilde{F} * k_d\right\}} \tag{13}$$

where k_d is the convolution kernel. The purpose of the convolution blurring is to reduce the sharpness of the peaks of *F* so that the resulting spatial filter $\tilde{F}'$ is less sensitive to precise locations of cross-polarization. To implement the filter $\tilde{F}'$, simple dot multiplication of the of the sum of the co-polarization images with the filter image is performed to yield the vampire signature image, I_{vamp} which accentuates points that correspond to low cross-polarization and dampens regions that correspond to high cross-polarization. The new, filtered image is normalized to unity and is given as:

$$\tilde{I}_{vamp} = \left(\left|\tilde{I}_{hh}\right| + \left|\tilde{I}_{vv}\right|\right) \bullet \tilde{F}' \tag{14}$$

In order to achieve detection with this information, a simple threshold χ_{th}, $0 \leq \chi_{th} \leq 1$, is applied to the $\tilde{I}_{vamp}$ data whereby any points that exceed χ_{th} are considered to be a region of interest. The result is a binary image $\tilde{I}_{bin}$ consisting of zeros and unity valued "blobs" that denote the regions of interest. These binary "blobs" are then designated to be landmines. A flow chart of the decision process is shown in Figure 3.

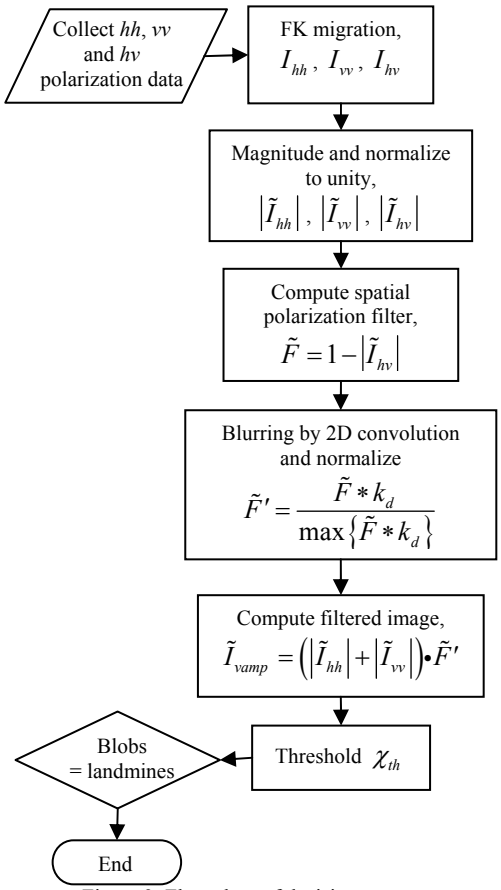

Figure 3: Flow chart of decision process

EXPERIMENTAL SETUP

The proposed GPR landmine detection method was tested in a controlled environment in a sandbox at the University of Manitoba. The sandbox, which is 1.2m wide, is filled to a depth of approximately 25cm of silica sand ($\varepsilon_r \simeq 2.5$) and the bottom of the sandbox is covered with a layer of absorptive RF foam to limit reflection from the bottom of the sandbox. The GPR system consisted of an Anritsu 360B vector network analyzer. Due to their good cross-polarization characteristics, two UWB Vivaldi antennas were used to take the measurements. The antennas were oriented 90° in space with respect to one another in order to capture the cross-polarization information. The operational bandwidth of the measurements was selected to be from 0.8GHz to 5GHz. All measurements along the synthetic aperture were made in 1cm increments along the radar path. The system setup and dimensions are shown in Figure 4.

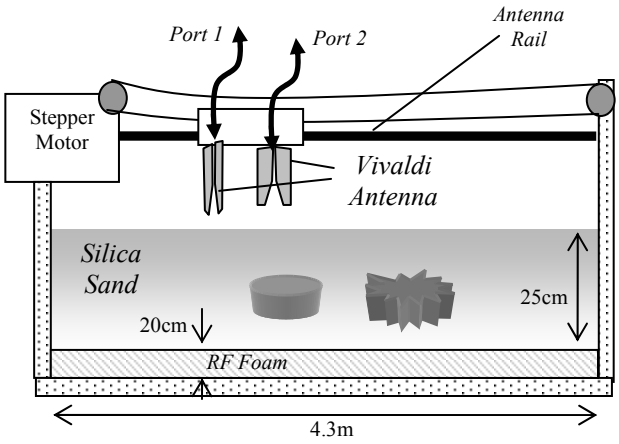

Figure 4: Experimental sandbox and GPR system

The targets used in the experiments consisted of cylindrical and rectangular shaped pieces of Styrofoam to simulate landmines, irregularly shaped pieces of scrap metal to simulate highly reflective clutter. The cylindrical Styrofoam mine-like targets measured 10cm in diameter and 3cm thick. The rectangular pieces measured 12cm × 5cm and were also 3cm thick. The metallic clutter targets were cut in irregular shapes from sheet metal and possessed approximate surface areas between 30cm^2 to 50cm^2.

EXPERIMENTAL RESULTS

To demonstrate the validity of the formulation, an example is presented as follows: eight Styrofoam mine-like targets, four cylindrical and four rectangular, along with four irregularly shaped pieces of metal (clutter) are embedded in the sand as shown in the top view diagram in Figure 5. The mine-like targets are oriented in a line so that their symmetry axes are all contained in a plane perpendicular to the air-ground interface so that a SAR measurement taken directly above the targets will result in the ideal circumstance whereby the bistatic antenna pair will be contained by all mine-like target symmetry planes. A SAR measurement taken directly above all the targets is then the identical situation discussed in [1]. A series of three SAR measurements are then taken. The first SAR measurement is taken directly above the targets, the second is taken along a SAR path parallel to the first, but shifted by 5cm and the third is shifted by 10cm as shown in Figure 6. The depths of the targets varied from 10cm to 13cm below the sand/air interface.

The normalized magnitude *hh* polarization image $\left|\tilde{I}_{hh}\right|$ for scan A is shown in Figure 7 along with $\tilde{I}_{vamp}$, where in both cases the effects of reflection from the air/ground interface have been time gated out of the image for the sake of clarity. The results are similar to those reported on in [1] and show that initially (before the method is applied) all targets exhibit responses that are difficult to

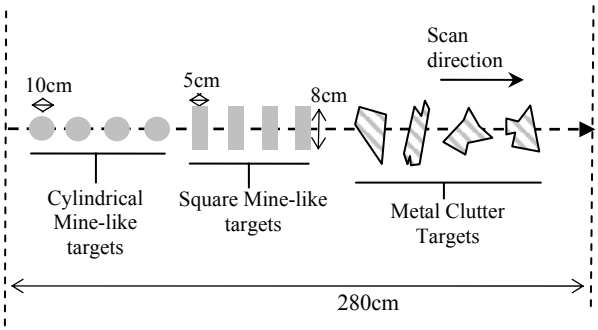

Figure 5: Top view of example experiment. Four targets are studied, two mine-like targets and two pieces of clutter

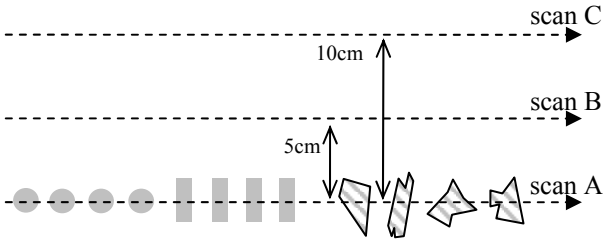

Figure 6: Top view of successive scans taken above the targets (scan A), shifted by 5cm (scan B) and shifted by 10cm (scan C).

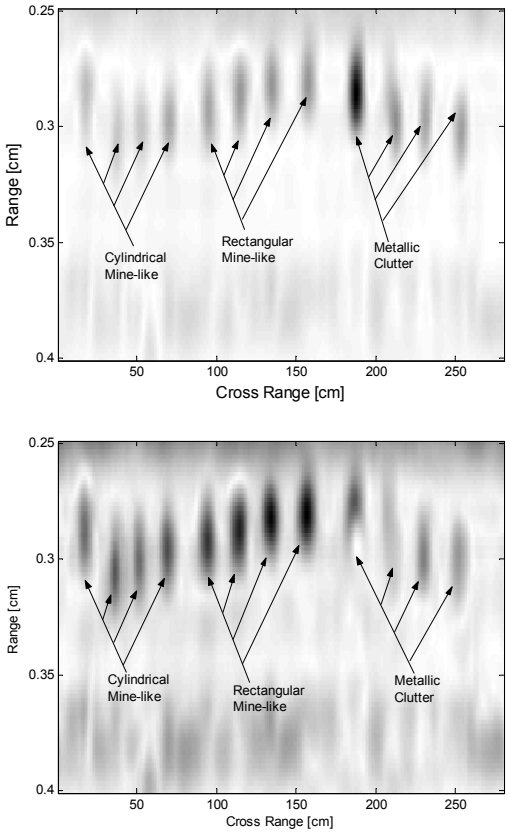

Figure 7: $\left|\tilde{I}_{hh}\right|$ (above) and $\tilde{I}_{vamp}$ (below) for scan A.

differentiate. The effect that the method has on the data is immediately evident since it can be seen that the filtered image exhibits strong responses from the mine-like targets relative to the clutter. The mine-like objects that have little

cross-polarization in their response are effectively amplified with respect to the clutter.

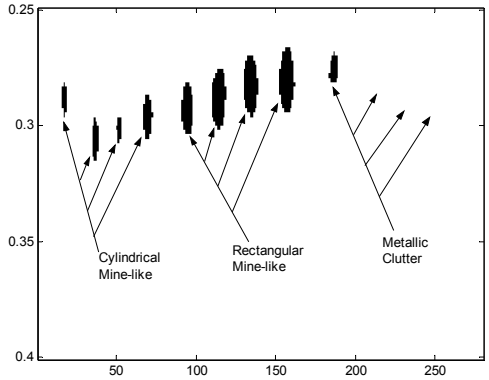

Figure 8: Binary image of scan A for a threshold of χ_{th} =0.6 showing successful detections of both mine-like targets.

The next step is to apply a threshold to the filtered image in order to obtain a binary representation of the vampire signature. Figure 9 shows the result of the application of a threshold value of χ_{th} = 0.6, which was determined to be optimal in [1] for the conditions of this experiment. All eight landmines are detected and one false alarm is detected.

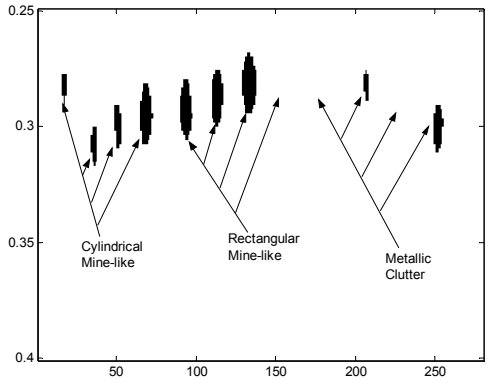

Figure 9: Binary image of scan B for a threshold of χ_{th} =0.6 showing successful detections of both mine-like targets.

In Figure 9, the resulting binary image for a threshold of χ_{th} = 0.6 is shown for scan B. Only seven of the eight landmines are detected and two false alarms are detected. Finally for scan C, the situation has deteriorated so much that no targets are detected at all. Rather than showing the blank binary image for this configuration, $\tilde{I}_{vamp}$ for scan C is shown in Figure 10 where it can be seen that the target responses for all 12 targets are very weak.

DISCUSSION AND CONCLUSIONS

The landmine detection algorithm based on the vampire signature proposed in [1] was subjected to subsurface mine-like and clutter measurements whereby the bistatic antenna pair were not necessarily contained within the target symmetry planes. The results show that the vampire

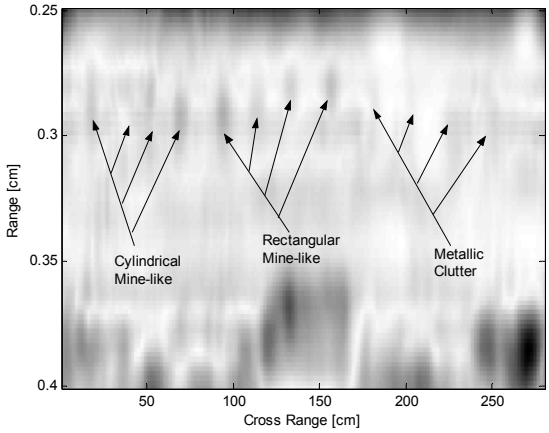

Figure 10: $\tilde{I}_{vamp}$ for scan C, the targets are all barely perceptible.

signature is very susceptible to variations in symmetry plane orientation with respect to the bistatic antenna pair. The results showed that the false alarm rate increases and the detection rate decreases for small deviations of the antennas from the symmetry plane (5cm) while the signature becomes virtually imperceptible for larger variations (10cm). Further research is required on a means to overcome, if not to take advantage of this apparent algorithmic flaw. An extension of the theory to SAR imagery in three dimensions is a direction that will be explored to this effect.

Despite the proposed method's susceptibility to deviations of the bistatic pair from the target symmetry plane, it should be noted that the cross polarization response still yields valuable information even when the bistatic pair are not contained in the target symmetry plane. For example, the information from successive SAR scans can be used in a methodological search for evidence of symmetry in the subsurface.

[1] M. Phelan, J. LoVetri, "Discrimination of Subsurface Targets with a Plane of Symmetry using Polarimetric Bistatic Radar", To be presented at the Tenth Int. Conf. on Ground Penetrating Radar, June, 2004, Delft, The Netherlands

[2] C. E. Baum, "Symmetry Analysis of Targets Near an Earth/Air Interface", *Interaction Note 554*, Air Force Research Laboratory (Directed Energy Directorate), March 1999

[3] C. E. Baum and H. N. Kritikos, *Electromagnetic Symmetry*. (New York), Taylor & Francis, 1995.

[4] J. F. Cornwell, *Group Theory in Physics*, Academic press, Harcourt Brace & Company, 1997

[5] J. M. Stiles et. al., "A group Theoretic Analysis of Symmetric Target Scattering With Application to Landmine Detection", *IEEE Trans on Geosci. & Remote Sensing*, Vol. 40, No. 8, Aug. 2002

[6] J. Gazdag, "Wave equation migration with the accurate space derivative method," *Geophys. Prospect.*, vol. 28, pp. 60–70, 1980.